Modeling Heterogeneous Photocatalytic Inactivation of *E. coli* Using Suspended and Immobilized TiO_2 Reactors

Majdi Kacem and Vincent Goetz
PROMES CNRS, UPR 8521, Rambla de la thermodynamique 66100 Perpignan, France

Gael Plantard
PROMES CNRS, UPR 8521, Rambla de la thermodynamique 66100 Perpignan, France

University of Perpignan Via Domitia, 52 Paul Alduy 66100 Perpignan, France

Nathalie Wery
LBE INRA, UR0050, Avenue des Etangs 11100 Narbonne, France

DOI 10.1002/aic.14834
Published online May 7, 2015 in Wiley Online Library (wileyonlinelibrary.com)

A study was carried out to develop a kinetic model of the photocatalytic inactivation of Escherichia coli using different TiO_2 catalysts. The model developed is based on a reaction scheme that involves effectively coupling mass-transfer fluxes between bacteria and catalyst surface on one hand and bacterial degradation reaction on the other. The photocatalytic results were derived from experiments led in a batch reactor under both dark and Ultra Violet (UV) irradiation conditions. Using a reference catalyst, the robustness of the developed model was tested under solar conditions. The experimental data validated the model as successfully able to reproduce evolutions in the viable bacteria concentration in the range of parameters studied without any further adjustment of the kinetic parameters. The model was used to simulate the bacterial degradation kinetics under different working conditions to describe the partitioning of both bacterial adhesion and photocatalytic reaction in the solution to be treated © 2015 American Institute of Chemical Engineers
AIChE J, 61: 2532–2542, 2015
Keywords: photocatalysis, kinetics, disinfection, titanium dioxide, adhesion, Escherichia coli

Introduction

Among the processes currently in development, semiconductor photocatalysis has emerged as a very attractive environmentally friendly water disinfection technology, especially as it can use solar power to drive the process.[1–4]

From a sustainable development perspective, the possibility of combining solar ultra violet (UV) irradiation and a stable semiconductor makes photocatalysis one of the most promising advanced oxydation treatment (AOT) for water disinfection.[5] However, sunlight is a discontinuous resource, which is a major constraint to factor into efficient design and running of the operating process. The industrial design and scale-up of photocatalytic disinfection technologies, therefore, needs a simulation tool capable of predicting how the process works on variable time and irradiation scales.

Literature reports on photocatalytic disinfection have focused on modeling the inactivation of different kinds of microorganisms,[6–9] including *Escherichia coli* which is, by far, the most studied organism in the world.[5,10] In most cases, disinfection profiles are successfully described by empirical models that are mathematical expressions aimed at replicating the observed behavior of inactivation curves[11–13] or by mechanistic models such as "Langmuir-type" interaction models[13,14] that tend to be more robust than empirical models. However, a major challenge when applying such models to disinfection is the difficulty in resolving microbe–catalyst interactions, particularly given their relative sizes and bacterial complexity. This means that even mechanistic models are simplifications that often require empirical approaches to complete them. To the best of our knowledge, few studies have been specifically performed to determine the kinetics of adsorption or, to use a more appropriate term, adhesion of microbes to the photocatalyst used.[15] Moreover, while a straightforward modeling approach may be desirable, simplistic formulations tend to neglect key process factors such as light intensity. Thus, it would appear that bacterial adhesion on the catalyst used as well as the light intensity at the catalyst surface should be an integral part of the bacterial inactivation model. In this context, this work focused on the kinetic modeling of the photocatalytic inactivation of Gram-negative *E. coli* bacteria using three titanium dioxide catalysts differing in size, structure, and other characteristics. The developed model is based on effectively coupling the mass transfers between bacteria suspended in the liquid bulk and the catalyst surface on one hand and the photocatalytic

Additional Supporting Information may be found in the online version of this article.

Correspondence concerning this article should be addressed to M. Kacem at majdi.kacem@promes.cnrs.fr

© 2015 American Institute of Chemical Engineers

degradation reaction on the other. For each of the solids used, the first step was to derive the reaction rate parameters and show how they can be measured from experiments carried out in a batch reactor under variable controlled light flux densities. To test the robustness and the fitness of the developed model, additional experiments were carried out using a reference catalyst under variable total treatment volumes and under real solar conditions. The aim of this second step was to demonstrate the ability of the kinetic model to simulate the performance of a large-scale reactor working under variable solar light flux densities without any further adjustment of the kinetic parameters, and thus, to demonstrate its suitability for use as a scale-up tool. Finally, the validated model was used to simulate the kinetics of bacterial degradation under different working conditions. The emphasis was on describing the partitioning of both bacterial adhesion and photocatalytic reaction in the solution to be treated and on gaining deeper insight into the contribution of each of solid and liquid phase to the total decrease in bacteria during the photoprocess.

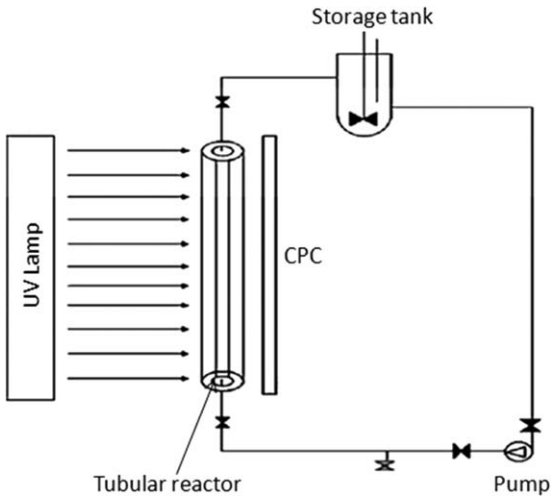

Figure 1. Laboratory set up.

Experimental

Materials

The media tested here have been studied in earlier works.[16,17] Two different TiO_2 aeroxides and a supported TiO_2 catalyst were investigated. The two aeroxides were (1) Degussa P25 (20–30 nm primary particle size by transmission electron microscopy (TEM); 54 $m^2\ g^{-1}$ specific surface area by Brunauer, Emmett and Teller (BET); 78% anatase, 22% rutile by x-ray diffraction) and (2) VP Aeroperl P25/20 (20–30 μm primary particle size by TEM; 46 $m^2\ g^{-1}$ specific surface area by BET; 80% anatase, 20% rutile by x-ray diffraction). The supported catalyst consisted in Millenium PC-500 immobilized on a flat cellulosic fiber support (98 $m^2\ g^{-1}$ specific surface area, 38 g m^{-2} cellulosic fibers, 16.7g m^{-2} TiO_2, 2 g m^{-2} Zeolite and 13.3 g m^{-2} SiO_2).

Bacterial strain and growth

E. coli strain DSM 30083 was used for the full bacterial inactivation study. This widely studied lab strain with a sequenced genome is a nonpathogenic primary model organism for lab research. *E. coli* cells were grown in sterile conditions in 0.1 L of Luria Bertani (Miller's LB Broth) medium at 37 °C.[18] Bacterial growth was monitored by optical density (600 nm) in a spectrophotometer (UVmini-1240, Shimadzu). Cultures in stationary phase were appropriately diluted in a buffer solution (buffered sodium chloride peptone water, pH 7.0, Oxoid) to obtain targeted initial bacterial concentrations.

For all studies, the efficiency of photocatalysis treatment on *E. coli* inactivation was evaluated, using a culture technique, the 4-méthylumbelliféryl-β-D-glucuronide (MUG)/*Ecoli* microplates, in accordance with the requirements of standard NF EN 9308-3-1999.[19] The bacterial inactivation, evaluated in most probable number per unit of volume (MPN L^{-1}), refers then to the loss of the cells culturability, which means the loss of their capability to grow on the culture media used.

Photoreactors and photocatalytic treatment

The model developed in this article involved effectively coupling photon flux density at the surface of the semiconductor and mass-transfer fluxes between the suspended bacteria and the catalyst surfaces. Thus, it was essential to investigate bacterial adhesion on the catalyst surfaces under dark conditions and to know the influence of UV flux density on the bacterial degradation reaction to simulate the bacterial profile as a function of irradiation time. Hence, two experimental installations were used. The first process is to carry out investigations under controlled conditions (dark and artificial irradiation) to establish the kinetic models representative of the inactivation of the target bacteria. The second process is to validate the simulations done with solar radiation.

The first laboratory set up shown in Figure 1 has been detailed previously.[20,21] The reactor was a cylindrical borosilicate glass tube (external diameter = 0.012 m, wall thickness = 0.0015 m, length = 0.8 m) operating in a closed recirculating circuit with a stirred reservoir tank, giving a total working volume of 1 L. Radiation source was a ultra violet A (UVA) lamp (VL-330) emitting at wavelengths centered at 365 nm. The radiation flux at the reactor axis was controlled at between 5 and 35 W m^{-2}. To illuminate the total surface of the reactor, an aluminum compound parabolic collector (CPC) was positioned just behind the reactor.[22] This parabolic mirror (concentration ratio = 1) comprised an aluminum sheet polished to deliver 95% reflectivity in the UV window. Both dark and photocatalytic experiments were carried out in the first laboratory set up. Under dark conditions, the adhesion experiments were investigated at different initial bacterial concentrations in the range 10^4 to 10^{10} MPN L^{-1}. Under UV light conditions, bacterial concentration was fixed at 10^7 MPN L^{-1} and the experimental data were obtained under variable light flux densities in the range 5–35 W m^{-2} corresponding to solar UV irradiation. Whatever the working conditions, the bacterial suspension exposed to the powdered catalysts flowed through the reactor by means of a volumetric pump and was continuously mixed in the recirculation tank.

Using the immobilized catalyst, the material was wrapped around a rod (diameter 0.005 m) and positioned at the axial center of the reactor, giving a total working surface of 0.02 m^2. The bacterial suspension flowed under laminar conditions through the annular space of the reactor, which corresponds to the ring-shaped space between the internal wall of the reactor tube and the glass rod fitted in place. Temperature and pH values were almost constant over time, at 25 °C and 6.9, respectively.

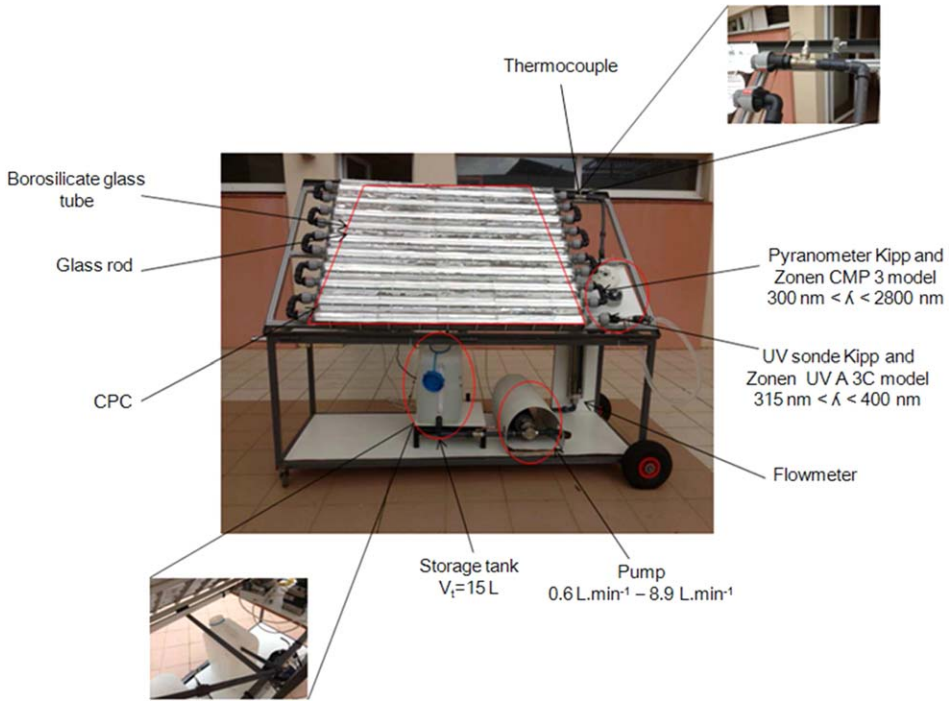

Figure 2. Solar plant.

[Color figure can be viewed in the online issue, which is available at wileyonlinelibrary.com.]

Throughout all experiments, samples of 18 mL volume were taken at regular intervals to monitor the time-course drop in bacterial concentration irrespective of the catalyst used. Thus, the catalyst first had to be separated from the samples to be analyzed. When using supported material, the samples were obviously catalyst-free. When using catalysts in powder, under the working pH (6.9 mostly neutral), the catalysts and microbes particles adhered, coflocculated and rapidly settled out of solution. In fact, the TiO_2 particles were close to the point of zero charge[23] and did not, therefore, experience significant repulsion from the mostly negative bacterial surface.[15]

To confirm the bacterial adhesion aspect relative to the catalysts used, samples from dark experiments were taken within 30 min of catalyst contact, fixed on hydrophilic polypropylene supports, washed with Milli-Q water, and dehydrated at room temperature. The samples were then sputter-coated with a 60% gold/40% palladium mixture, and analyzed under a Hitachi S-4500 model scanning electron microscope (SEM).

It was essential to study photocatalysis in experiments using the small-scale pilot set up in the lab to develop a general kinetic law representing the functioning of photocatalytic media in controlled irradiation conditions. Hence, the subsequent solar experiments carried out in real-life conditions were essential to verify whether the modeled kinetics really does account for the responses of bacterial photocatalysis when working (1) under larger scale (different residence time of the solution to be treated) and (2) under discontinuous solar irradiation.

To check model validity and robustness under these conditions, additional experiments were undertaken using the powdered P25 catalyst, which is widely considered as the benchmark for photocatalytic processes. The first additional experiment was conducted in the indoor experimental set up and carried out with different total volumes to be treated in the range 0.5–5 L, which corresponds to residence times ranging from 18 to 1.8% of total treatment time. The photocatalysis started at a fixed bacterial concentration equal to 10^7 MPN L^{-1} under 35 W m^{-2} of light flux density. Temperature and pH were kept constant over time, at 26 °C and 6.8, respectively.

Like the indoor experiment, the second additional experiment was operated in a batch mode and conducted outdoors in a solar set up. The pilot is shown in Figure 2 and detailed elsewhere.[16] It was composed of a tubular CPC reactor made up of 10 borosilicate glass tubes (external diameter = 0.032 m, wall thickness = 0.002 m, and length = 1.5 m). The CPC-type reflectors made of polished aluminum were placed under the tubes forming the reactor to ensure that light reaching the tube surfaces was homogeneous.[24] The exposed surface of each CPC was 0.14 m^2, thus providing 1.4 m^2 of total surface area exposed to solar radiation. The volume of the irradiated reactor was 10 L and the total volume of the fluid loop equaled 15 L. The solar investigations were carried out under UVA irradiation condition. The light flux density in the UVA spectral range I_r (W m^{-2}) was measured through a UV probe, which recorded the spectral range from 310 to 400 nm. In fact, this spectrum corresponds to the irradiation range effective for photocatalytic reaction. The global irradiation measurements were made with a pyranometer (Kipp & Zonen type CMP 6) covering a spectral range from 310 to 2800 nm. The solar experiment was performed in Perpignan (42°41′N, 2°53′E). The pilot, tilted at 42°, was faced south. The experiment started on a cloudy day with a maximum UV flux density of 23 W m^{-2} and at an initial concentration of 10^7 MPN L^{-1}. The bacterial suspension exposed to the TiO_2 slurry was mixed continuously in the tank, fed into the reactor with a pump, and recirculated to the storage tank. The same sampling and bacterial analysis protocols were maintained throughout this experiment. Temperature was monitored over time in the range between 20 and 40 °C, and pH was constant at around 7.

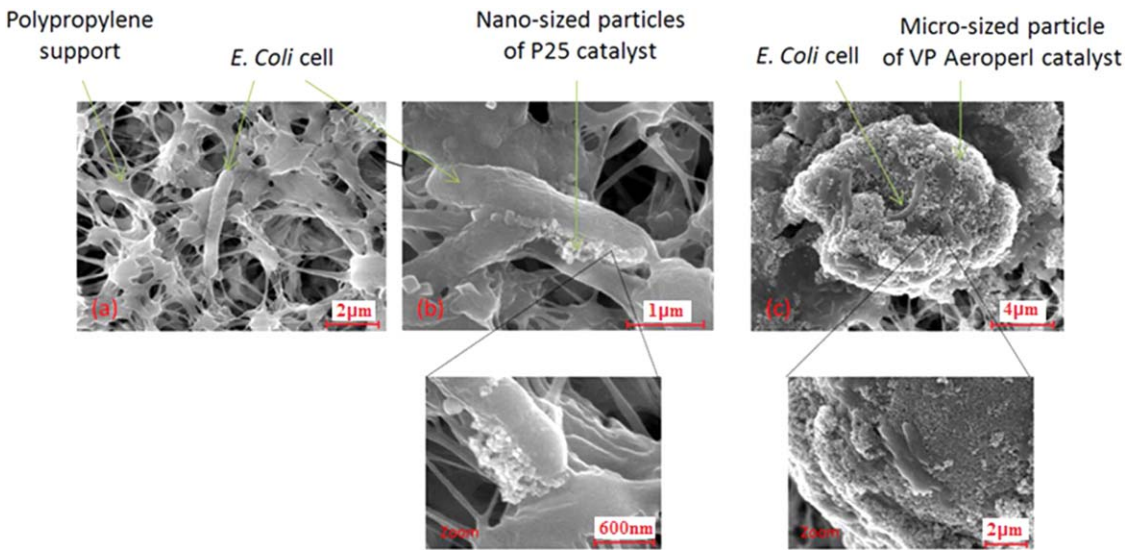

Figure 3. SEM images of suspended *E. coli* cells under dark conditions.

(a) without catalyst particles, (b) within 30 min of contact time with the P25 catalyst, (c) within 30 min of contact time with the VP Aeroperl catalyst. [Color figure can be viewed in the online issue, which is available at wileyonlinelibrary.com.]

Results and Discussion

Adhesion experiments

This article presents a theoretical model for photocatalytic disinfection that accounts for bacteria–catalyst interactions. The literature has already demonstrated the feasibility of *E. coli* photoinactivation by heterogeneous photocatalysis[9,18,25,26] and *E. coli* adhesion on solid materials.[15,27,28] The aim here was essentially to obtain experimental data under different controlled working conditions to identify the unknown parameters involved in the kinetics of bacterial degradation and to validate the model (presented in the next section) under real solar conditions. Hence, quantitative analysis of the bacterial adhesion on the catalysts surfaces and subsequent chemical photocatalytic degradation reactions are important to model the overall bacterial disinfection process. To confirm the bacterial adhesion aspect relative to each catalyst, samples taken during adhesion experiments were analyzed within 30 min of catalyst contact time by SEM.

The SEM pictures obtained using each of the catalysts are shown in Figure 3. The pictures were representative of the samples observed on the microscopic sampler-holder. The rod-shaped morphology of the approximately 3 µm long and 0.7–0.8 µm wide *E. coli* cell in absence of catalyst is shown in Figure 3a as control. The cell displayed a smooth continuous outer membrane appearance and was shown to be intact in the buffer solution used. Within 30 min of contact time with the TiO_2 nanoparticles (Figure 3b) and microparticles (Figure 3c), the cells retained their general morphology, which is interesting in that it highlights that TiO_2 has a neutral catalytic effect on bacteria under dark conditions.

From a particle-size perspective, the interaction between the catalysts used and the target bacteria was viewed in two ways. In the first case, the P25 particles with a large 20-nm diameter were much smaller than the cell, and several catalyst particles were attached to the single cells. However, in the second case (c), VP Aeroperl particles were almost 10-folds bigger than *E. coli* cells, and a large number of microbial cells were attached to external particle surfaces. The same phenomenon was seen when using the supported catalyst.

In this work, we admit that the bacterial adhesion is due essentially to a physisorption of the cells membranes to the catalysts surfaces. In fact, under the pH condition of interest (6.9, i.e., mostly neutral), the TiO_2 surface is dominated by noncharged surface hydroxylated species, while the cell surface is mostly negative. Thus, it is easy to see that under the given conditions, TiO_2 would not experience significant repulsion from the bacterial surface because the particles are close to the point of zero charge. Therefore, adhesion between the TiO_2 and the bacterial cells will mostly be governed by short-range van der Waal forces.

Once the bacteria–catalyst interaction aspect was confirmed, the next step was to quantify colloidal bacterial adhesion. Results of adhesion experiments were obtained under dark conditions and at different initial concentrations in the range 10^4 to 10^{10} MPN L^{-1}. The profiles obtained for each of the catalysts depict the decrease in bacterial concentration in the liquid bulk (MPN L^{-1}) as a function of catalyst contact time (min), and were closely mirrored. Figure 4 illustrates the case of the powdered P25 catalyst used in the first instance. Results obtained using the microparticles and the supported catalysts are shown in Figures A1 and A2, respectively (see Appendix).

Using the P25 catalyst, and in the range of concentrations studied, the obtained kinetics displayed almost the same profiles, with a low initial bacterial decrease in the fluid bulk due to bacterial adhesion, then reaching an asymptotic limit (C_e) at the end of the experiment. This steady state, at which point the net change in concentration is practically zero ($<10^{-1}$), corresponded to an equilibrium state taking place between the solid and the liquid bulk.[29] In the case of the supported material, the constant concentration observed in the liquid bulk at the equilibrium stat traduces obviously the constant bacterial density on the material surface. This result is interesting so far as it highlights the neutral effect of the catalyst as well as the cellulosic matrix constituting the two-dimensional (2-D) material under dark condition.

At the equilibrium state, and in the range of concentrations studied, the bacterial mass balance made it possible to

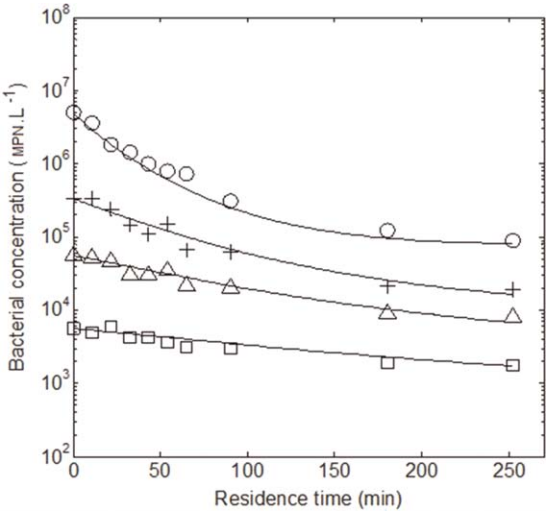

Figure 4. Adhesion kinetics of *E. coli* over residence time using the suspended P25 catalyst and for different initial bacterial concentrations.

determine density of the bacteria attached on the catalyst surfaces, q_e. Given the different shapes and sizes of the catalysts used, it was decided to select the total surface of the photocatalytic solids as reference to express the amount of attached bacteria. Hence, q_e was expressed as number of attached cells per unit of total catalyst surface (MPN m^{-2}). For each of the catalysts used, the adhesion equilibrium curves plotted, which express q_e (MPN m^{-2}) as a function of C_e (MPN L^{-1}), are shown in Figure 5.

In the range of concentrations studied, the obtained profiles corresponded to the following slightly modified *Freundlich* Eq. 1

$$q_e = F \cdot C_e^{\frac{1}{n}} \quad (1)$$

where F and n are model parameters (dimensionless). The obtained parameters of this Freundlich equation are given in Table 1.

Following Eq. 1, the adhesion equilibrium profiles produced by the two powder-suspension catalysts showed similar curve profiles, indicating that they deliver practically identical performances in terms of bacterial adhesion. These

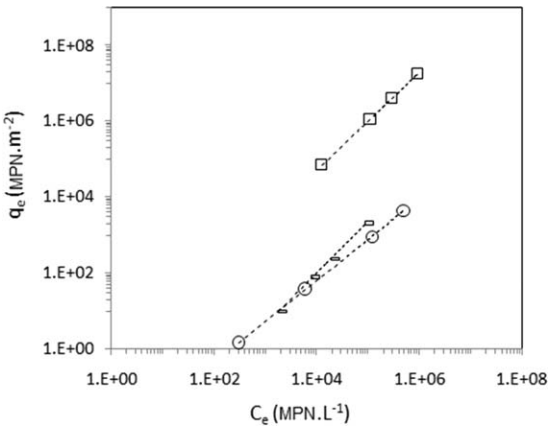

Figure 5. Adhesion equilibria of *E. coli* using P25 catalyst in suspension (□), VP Aeroperl catalyst in suspension (○), and 2D material (□).

Table 1. Parameters Identified for the Freundlich Model

Media	F	n
P25	0.014	0.74
Aeropert	0.1	0.92
Supported catalyst	31	0.78

two suspension-format media shared the same type of catalyst submitted to the same fluid flow conditions, and their only distinguishing factor was their specific surface area which was shown to be a nonimpacting factor since cells attached were expressed per unit of total surface of catalyst. In contrast, as illustrated in Figure 5, the suspended catalysts adhesion capacities were outperformed by the 2-D media (factor >100), most probably due to its nanocrystallite composition and its different cellulosic structure. These results confirm how structure and nanocrystallite composition of the catalyst inside the photoreactor volume are defining factors shaping the ultimate bacterial adhesion performances of a given material.

Photocatalytic experiments

Results of photocatalysis using each of the catalysts were recorded under variable irradiation conditions corresponding to the solar UV range. The photocatalytic disinfection kinetics were experimentally established for each media preconfigured to reach 99% absorption of available light.[21] This means that the amount of light energy absorbed by the media equates to 0.99-folds the amount of light energy incident on the photoreactor surface. The aim here is to define an optimal configuration for each catalyst that ensures the maximum absorption of UV irradiation entering the reactor, the geometry of which defines the optical path length of the emitted light. Based on a previous study,[21] this configuration ensured the highest bacterial degradation reaction rate.

The profiles obtained depict the decrease in bacterial concentration in the liquid bulk (MPN L^{-1}) as a function of residence time (18% of total treatment time [min]).

As for the above dark experiments, Figure 6 presents the case of the powdered P25 catalyst used in the first instance. The results obtained using the microparticles and the supported catalysts closely mirrored those obtained by the P25 catalyst and are shown in Figures A3 and A4, respectively (see Appendix). The bacterial degradation was monitored only in the liquid phase irrespectively to the catalyst used. Thus, beforehand each analysis, a separation of the catalyst from the solution was carried out. Hence, the detected bacterial decrease under dark condition (Figure 6) is due to the transfer of the cells from the liquid phase to the solid one which is referred to the bacterial adhesion phenomenon. Under irradiation condition, this decrease was enhanced even more by photocatalytic reaction.

The presence of the attached bacteria on the catalyst surface did not seem to inhibit the light absorption by the catalyst and so its reactivity. This, could principally be due to (1) the well transmission of UV light of the bacteria in the spectral range studied (result not shown) and (2) to the low recovery rate of bacteria on the catalyst surface. In fact, the total surface of bacteria initially present in the liquid (10^{-5} m^2, which is calculated as the product of the average surface of one *E. coli* cell and total bacterial cells) equates only 10^{-2}-folds the total active surface of the catalyst introduced into the reactor.

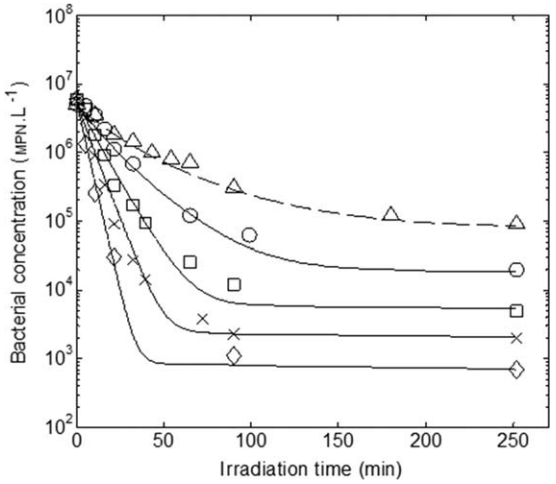

Figure 6. Experimental and simulated results of the photocatalytic inactivation of *E. coli* over irradiation time using the suspended P25 catalyst under variable artificial irradiation flux densities.

0 W m^{-2} (Δ), 5 W m^{-2} (○), 10 W m^{-2} (□), 20 W m^{-2} (×), and 35 W m^{-2} (◇).

The profiles obtained showed the effect of increasing activity for higher irradiation power. In fact, the plots showed two different bacterial inactivation regimes: a log-linear inactivation regime dependent on radiation flux density, and a final deceleration process. Using data from the first region of the inactivation curves, the calculated T_{90}, which stands for the time for 90% decay showed a maximum value of 60 min whatever the light flux density is.

However, the catalyst was unable to achieve total bacterial disinfection over treatment time, and reached an asymptotic limit of inactivation. This is known by the tail, and could be related, as reported in literature,[14,30] to target bacteria developing resistance during the disinfection treatment or to an inhibition phenomenon produced by competition with organic products released to the medium, as explained elsewhere.[31]

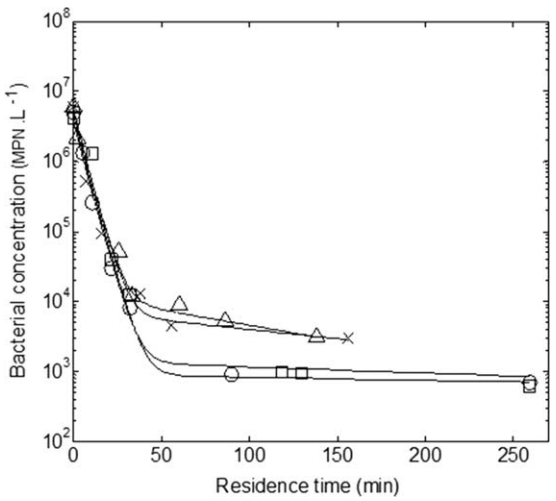

Figure 7. Experimental and simulated results of the photocatalytic inactivation of *E. coli* over irradiation time using the suspended P25 catalyst for different total volumes to be treated.

0.5 L (○), 1 L (□), 3 L (×), and 5 L (Δ).

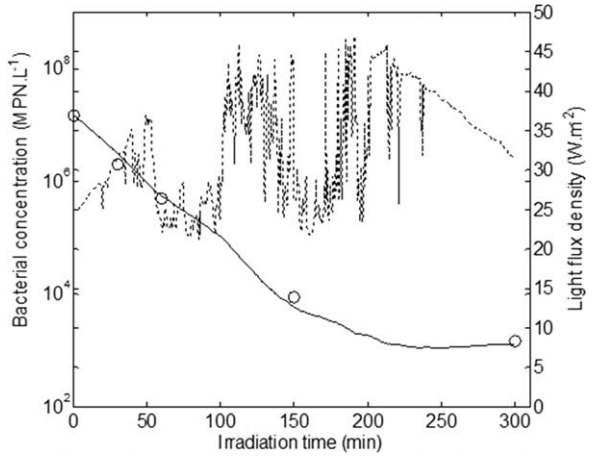

Figure 8. Experimental (○) and simulated (continuous line) results of the photocatalytic inactivation of *E. coli* over time under solar light flux densities and using the suspended P25 catalyst.

Conversely, additional photocatalytic experiments carried out under variable total treatment volumes (Figure 7) and under solar irradiation (Figure 8) showed an expected effect of increasing activity for higher irradiation time and longer times required to treat higher volumes. Moreover, in the range of the total volumes to be treated (from 0.5 to 5 L), the residence time parameter did not seem to be an impacting factor on bacterial degradation kinetics as the obtained profiles had almost merged. This suggests that the bacteria did not develop resistance to the photocatalytic treatment during its dark-phase stay in the storage tank. Moving on from these conclusions, the next step—and the main goal of this study—was to obtain the values of the kinetic parameters that best reproduce the photocatalytic activity results with the model developed (see the next section) and to validate it under real-world conditions.

Derivation of the kinetic model

There have been few attempts to define specific models for photocatalytic disinfection, as most of the current applications are based primarily on chemical disinfection. Water disinfection modeling began as a purely empirical science based on the principles expressed in Chick's law.[11] Chick observed that under certain conditions, microorganism inactivation kinetics closely mirrored chemical reactions. The fundamental laws governing chemical reaction kinetics were thus applied to reactions involving microorganisms and a chemical disinfectant. The kinetic law most frequently used is the pseudofirst-order law relating to contaminant concentration in which the value of "constant" k is directly proportional to irradiation I.[32] Some authors have suggested generalizing the pseudofirst-order kinetics by establishing a power function of the irradiation intensity.[33,34] However, at the present time, there is no universal kinetic law able to represent the complex photocatalytic mechanism that is basically dependent on local irradiations that dictate the speeds at which radicals are formed. The most simplified mechanism described so far in literature is that the photocatalytic reaction proceeds at the semiconductor surface and is the result of three steps: (1) production of electron–hole pairs by

irradiation of TiO_2 with photons whose energy is higher than the band gap energy of the semiconductor; (2) formation of highly reactive radicals, and (3) reaction between the photogenerated radicals and the target bacteria. Thus, even there is still much debate over which process leads to the inactivation of *E. coli* once exposed to photocatalytic action, it is admitted that the destruction of the cell membrane due to the oxidative radical attacks is the most important process. Consequently, the degradation of the bacterial membrane, main actor in the bacterial adhesion process, might lead to the desorption (detachment) of the cell from the catalyst surface.

Although there is still some debate over whether radicals react with bacteria in the fluid bulk phase or with bacteria attached at the photocatalyst surface, both options are acceptable mechanisms.[35–37] In fact, during the illumination of TiO_2 particles, radicals are produced at the catalyst–water interface. The generation of the radicals is central to the overall photocatalytic process.

Looking at the literature, there are two theories on the nature of the radicals at the catalyst surface: (1) radicals remain surface-bound to the catalyst during reaction with adsorbed species[38,39] and (2) radicals diffuse away from the surface to react with compounds in solution or on the catalyst surface.[35,36,40] Therefore, radicals could potentially diffuse into a bacterial membrane if they get very close to a catalyst surface. Hence, it could be accepted that once the target bacteria is transferred to the catalyst surface, the photocatalytic reaction would likely degrade the bonded bacteria as well as the bacteria in very close proximity to the catalyst surface. Consequently, the couplings between mass transfer of bacteria from the liquid bulk to the catalyst surface, the adhesion phase, and the "intrinsic" photocatalytic degradation reaction all have to be taken into account in any model of global bacterial decrease during the photochemical treatment process.

Considering that the surface adhesion rate for physical adhesion is rapid enough to be assumed as instantaneous relative to transfer across the fluid film around the particle, the flux density of bacteria transferred to the very close proximity of the catalyst surface could be expressed by Eq. 2[20]

$$\mathrm{N} = -K_s \,.(q_e - \mathrm{q}) \tag{2}$$

where N is flux density of bacteria transferred (MPN m^{-2} s^{-1}) from the bulk solution to the solid surface, K_s is fluid film mass-transfer coefficient (s^{-1}), q is attached phase concentration and q_e (given by Eq. 1) is attached phase concentration in equilibrium with the bulk solution phase, both of which are expressed as number of attached bacteria per unit of m^2 of catalyst surface (MPN m^{-2}).

Conversely, as described elsewhere,[20,41,42] the "intrinsic" degradation rate "ṙ" could be considered a first-order kinetic law according to the amount of target contaminant (e.g., bacteria) to be degraded. Moreover, it has been demonstrated in the literature[33,34] that the photocatalytic reaction constant "k" could be generalized by establishing a power function of the irradiation intensity. Considering that this dependence is regardless of whether the target contaminant it a chemical molecule or bacterial cell, the reaction rate for the inactivation of both bacteria transferred to the very close proximity of the catalyst and bacteria bounded to the catalyst surface could be expressed via Eqs. 3 and 4, respectively

$$\dot{\mathrm{r}} = \mathrm{k} \,.\, \mathrm{C} = \left(\alpha \,.\, I_r^{f}\right).\mathrm{C} \tag{3}$$

$$\dot{\mathrm{r}} = \mathrm{k}' \,.\, \mathrm{q} = \left(\alpha' \,.\, I_r^{f'}\right).\, \mathrm{q} \tag{4}$$

where k and k' are bacterial degradation rate constants (s^{-1}) dependent on the production of the oxidative radicals, which in turn is assumed to be dependent on the UV irradiations absorbed into the reactor volume, C is bacterial concentration in the fluid bulk phase (MPN L^{-1}), q is bacteria bonded to the catalyst surface (MPN m^{-2}), α and α' ((m^3 J^{-1})$^{-f}$) are energy constants related to semiconductor activity, and f, f' (dimensionless) are coefficients that reflect the influence of the light on the bacterial degradation rate.

Assuming that the optical properties of the suspension do not vary during the reaction (no formation or disappearance of absorbing species nor significant changes in pH value that could modify the aggregation of the catalyst particles), the averaged irradiation I_r (W m^{-3}) into the reactor can be considered to be constant over treatment time and could thus be used to evaluate the average reaction rate inside the reactor total volume.

To represent the dynamic behavior of the recirculation reaction system under variable irradiation conditions and using the P25 catalyst in the first instance, the species balances have to be considered for both suspended bacteria transferred to the very close proximity of the catalyst surface (Eq. 5) and bacteria bonded to the catalyst surface (Eq. 6).

Considering that (1) the mass transfer occurs in the overall volume of the loop and (2) the photocatalytic reaction occurs only in the irradiated volume V_r (L), and taking into account the equivalent surface of the catalyst per unit of total volume to be treated S_{cat} (m^2 L^{-1}), the material balances yield the following differential Eqs. 5 and 6

$$\frac{dC}{dt} = -K_S \cdot S_{cat} \cdot (q_e - q) - \frac{V_r}{V_t} \cdot \alpha \cdot I_r^{f} \cdot C \tag{5}$$

$$\frac{dq}{dt} = K_S \cdot (q_e - q) - \frac{V_r}{V_t} \cdot \alpha' \cdot I_r^{f'} \cdot q \tag{6}$$

The bacterial inactivation by photocatalysis is described in the liquid phase (Eq. 5) as well as in the solid phase (Eq. 6) by coupling the mass transfer of the bacteria (Eq. 2) and the subsequent photocatalytic reaction depending on the irradiation (Eq. 3 in the liquid phase and Eq. 4 in the solid phase). The material balances work to the assumption that the axial concentration gradient inside the tubular reactor can be considered negligible.

Basically, solving the system of differential equations regardless of the irradiation conditions provides the concentration profiles of bacteria in the liquid phase C (MPN L^{-1}) and the density of bacteria q (MPN m^{-2}) in the solid one as a function of the residence time (irradiation time) of the solution to be treated in the photocatalytic reactor t_r (s) (expressed by Eq. 7).

The in-dark experiment (e.g., bacterial adhesion) corresponds to the special case of an irradiation I_r equal to 0 W m^{-2} (shown in Figure 6). The differential equations corresponding to both cases of microsized and supported catalysts are shown in the Supporting Information

$$\mathrm{t_r} = \mathrm{t}.\frac{\mathrm{V_r}}{\mathrm{V_t}} \tag{7}$$

where t is total treatment time (s).

Table 2. Kinetic Parameters Identified for Photocatalytic Inactivation Modeling

Matériau	S_{cat} ($m^2\ L^{-1}$)	K_s ($10^{-6}\ s^{-1}$)	α ($10^{-6}\ m^3\ J^{-1})^{-f}$	f	α' ($10^{-6}\ m^3\ J^{-1})^{-f'}$	f'	MRE (%)
P25	82	0.61	12.5	1.2	3.02	0.36	8.5
VP aeropert	116.2	1.6	12.7	1.4	34	0.0013	10
Supported catalyst	0.013	2.16	10.2	1.2	19.47	0.064	9.8

Kinetic parameters

Apart from the experimental conclusions obtained, the goal of this work was to obtain the values of the kinetic parameters that best reproduce the photocatalytic activity results with the model developed and to better describe the intrinsic bacterial inactivation process under variable irradiation conditions. These parameters were identified using an optimization method (Optimization via Matlab) based on the minimization of the mean relative error via Eq. 8

$$\text{MRE}\ (\%) = \frac{1}{n}.\sum_{i=1}^{n}\left|\frac{C_{exp}\text{-}C_i}{C_{exp}}\right| \times\ 100 \qquad (8)$$

where n is number of data points and C_i and C_{exp} are the values predicted by the model and the experimental data, respectively.

For each of the catalysts used and in the range of bacterial concentrations studied, the value of the mass-transfer coefficient K_s was optimized to provide the best fit to the bacterial adhesion kinetics under dark conditions shown in Figures 4, A1, and A2. Figure 4 presents the result using the Degussa P25 catalyst with continuous line being the simulated concentration profile as function of the contact time.

The direct comparison of K_s values between the supported catalyst and the TiO_2 particles is tricky. Mass transfer of the bacteria arises in very different conditions, that is, a mass transfer between a liquid that flows in a laminar regime in an annular space and a cylindrical surface, which is taken as reference in the mass balance; a mass transfer from a liquid toward suspended particles that are agitated under different conditions (stirred tank and tubular reactor). In addition and in agreement with the linear driving force formalism adopted,[43] the K_s values could be also considered as the result of the coupling phenomena between mass transfer in the fluid film and adhesion at the surface or in the few pores near the surface of the catalyst. Finally, in the case of TiO_2 particles, it is necessary to keep in mind that mass transfer occurs between microorganisms and particles while the numerous studies and correlations available in the literature are established in the case of particles in contact with dissolved chemical species. Then, direct use of such correlations is not obvious. Nevertheless, with reference to one of the most complete and very often cited work performed by Barker and Treybal,[44] the mass-transfer coefficient, in the case of solids suspended in agitated liquids, has to be independent of particles size. The mass-transfer coefficients obtained for the Degussa P25 and Aeroperl VP do not strictly respect this constraint but it can be outlined that they are of the same order of magnitude with a ratio limited to 2.5 between the two identified values.

For a given catalyst, once the value of K_s determined experimentally, the values of α, α', f, and f' were subsequently optimized to provide the best fit to data obtained under variable irradiation conditions (Figures 6, A3, and A4).

Using each of the catalysts, it can be seen that the kinetic model fits the experimental results with a reasonable degree of accuracy, even though small deviations are observed (MRE $\leq$10%). Table 2 reports the identified parameters of the kinetic model. Based on the results obtained, parameters α and f were found to yield almost the same values. Using each of the catalysts, optimized values of α and f ($\sim$1) for the evolution of the kinetic "constant" k (I_r) as a power function of the light flux density indicates the direct proportional effect of this operating parameter on the photocatalytic degradation reaction in the fluid bulk. However, the optimized values of α' and f' now yielded significantly different values. In this case, the model showed the limiting effect of light flux density on the catalyst surfaces. This dependence of the kinetic constant k on the level of irradiation I_r in accordance with an irradiation power law ($f' < 1$) could be linked to recombining processes of the electrical charges, or a limitation due to the transfer of byproducts of photocatalysis on the catalyst surface.

Once we were able to complete the parameter identification stage using the results obtained under our different controlled conditions, the additional experiment led on different total volumes to be treated (Figure 7) and the solar experiment (Figure 8) were essential to test the robustness and reliability of the kinetic model. Taking into account the characteristics of the different set up, tank, and reactor volumes and irradiated catalyst surface, calculations were performed with the same kinetic formula. Note that no supplementary adjustment of α, α', f, and f' was done—the values previously determined for the four parameters involved in the kinetic law were directly used in the simulation. Once again, as clearly shown in Figures 7 and 8, the kinetic model fits the additional experimental results with a reasonable degree of accuracy. Hence, the agreement between the calculated and experimental concentration profiles during the entire course of the reactions under variable artificial irradiation, variable total residence time of the solution to be treated, and discontinuous solar irradiation validates the model for the photoprocess simulation and substantiates the necessity of including the coupling between both bacteria–catalysts interaction and photocatalytic reaction rate.

Intrinsic kinetic description

The results highlight that bacterial decrease in the fluid bulk can be governed by two main phenomena, that is, bacterial adhesion on the catalyst surface and the photocatalytic reaction rate which is dependent on the quantity of energy absorbed by the material. Accordingly, both kinetic regimes may coexist inside the reactor at more or less different order-of-magnitude rates. The objective of these simulations was thus to highlight the partitioning of these two phenomena in the suspension to be treated, that is, to describe the relative contribution of each phase (liquid phase and solid phase) to total bacterial decrease during the photodegradation process.

The profiles shown in Figure 9 deviated from the numerical integration of the Eqs. 5 and 6 led under both dark conditions and 35 W m^{-2} of irradiation power using the P25 catalyst in the first instance.

The numerical integration of the Eqs. 5 and 6 was performed for a total volume to be treated equal to 1 L, with the following conditions:

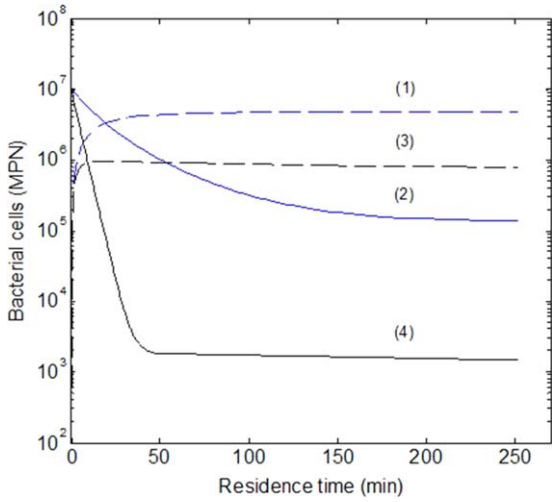

Figure 9. Simulated results of the photoinactivation of *E. coli* over irradiation time under dark conditions on the solid phase (1) and on the liquid bulk (2) and under 35 W m^{-2} light flux density on the solid phase (3) and on the liquid bulk (4).

[Color figure can be viewed in the online issue, which is available at wileyonlinelibrary.com.]

At $t = 0$

$$C = C_{init} = 10^7 (\text{MPN L}^{-1}) \quad (9)$$

$$q = q_{init} = 0 \ (\text{MPN m}^{-2}) \quad (10)$$

with C_{init} and q_{init} are the initial values of bacterial concentration in the liquid phase and the density of attached bacteria on the catalyst surface, respectively.

To depict the bacterial evolution in the liquid phase as well as in the solid one, the profiles were reported in bacterial MPN as function of the residence time. Curves 1 and 2 depict the MPN of bacteria under dark condition in the solid and liquid phase, respectively. Under light condition, the profiles of bacteria MPN in the solid and liquid phase corresponded to Curves 3 and 4, respectively.

Results under dark conditions showed a non-negligible interaction between target bacteria and catalyst used. In fact, 90% of total bacteria initially present in the liquid phase had bonded to the catalyst surface within only 10% of total catalyst contact time (Curve 1). In parallel, this adhesion induced a decrease in bacterial count in the bulk liquid until reaching a stationary phase (Curve 2) corresponding to equilibrium state. In this case, the calculated sum of both bacteria in the liquid and solid phases throughout the catalyst contact time corresponded to the number of bacteria initially present in the suspension.

Under UV irradiation conditions (black curves), the profiles obtained comprised two elementary steps. Up to 10% of total photocatalysis time (first step), there was almost a 1-log decrease in total bacteria initially present in the liquid phase (Curve 4). In parallel, there was a slight bacterial adhesion activity on the solid phase that represented almost 10% of total bacteria initially present in the suspension (Curve 3). These results tend to demonstrate that at the start of the treatment, the photocatalytic reaction activity in the liquid phase was of a higher magnitude than the adhesion activity. Then, beyond 10% of total photocatalysis time (second step), the bacterial decrease in the liquid phase proceeds in a one-way manner until reaching a stationary phase representing the tail phenomenon. In the same period, the degradation of the cells in the solid phase seems to be inhibited. In this case, it has to be cautioned that the log scale gives the impression that the number of bacterial cells is constant, whereas it actually varied from 10^6 cells to 2×10^5 cells over the 200 min of simulation time, recording thereby a degradation rate of 20%. Thus, although degradation is partially inhibited in the solid phase, it still proceed slowly during the photocatalytic process.

Given the results of this simulation, the partitioning of both photocatalytic activity and bacterial adhesion phenomena highlight that (1) the contribution of bacterial adhesion to global bacterial decrease in the bulk liquid generally has a lower magnitude than photocatalytic activity and (2) photocatalytic activity was of significantly lower magnitude on the solid phase than on the liquid phase.

We believe that the low impact of the photocatalytic reaction in the solid phase compared to the solution phase could be related to (1) a high recombining processes of the electrical charges formed at the catalyst surface, (2) a limitation due to a potential transfer of byproducts of photocatalysis on the catalyst surface, (3) a restrained mass transfer of oxidative radicals into microbial cells membranes at the direct contact of the catalyst surface, and (4) radicals diffusing in the liquid phase can combine with other chemical products to form additional reactive oxidative species that enhance the photocatalytic reaction, as reported elsewhere.[45]

However, although degradation was inhibited on the solid phase, it can still proceed slowly during the adhesion process. These results are interesting as they highlight the presence of a significant amount of viable bacteria on the catalyst surface at the end of the experiment and strongly suggest that the efficiency of heterogeneous photocatalysis for bacterial disinfection could be dangerously overestimated.

Conclusion

This study developed a kinetic model of the photocatalytic inactivation of Gram-negative *E. coli* using three titanium dioxide-based catalysts differing in size, shape, and other characteristics. This choice associated with an adapted reactor design enables effective coupling between two basic phenomena that coexist in the suspension to be treated—that is, bacteria–catalyst interaction and the photocatalytic reaction—to model the overall bacterial disinfection process. Our aim was not to develop an exact phenomenological model, which would need, among other requirements, the definition of a local rate provided by the resolution of the partial differential equation based on a radiation balance (to take into account the irradiation profiles inside the reactor). However, the objective was to build on the many studies already undertaken on the subject to suggest a global approach that, with reasonable simplifications and assumptions, would enable the development and validation of a simple, robust, but nevertheless representative model of the disinfection process.

The model has been successfully validated by experimental data, as it is able to reproduce the evolution in concentrations of viable bacteria in a wide range of artificial UV flux densities corresponding to solar irradiation. Next, the robustness and suitability of the model were validated under real solar irradiation conditions. The simulations of bacterial degradation given here, highlight a partitioning of the two studied phenomena in the suspension to be treated. This made it possible to understand the relative contribution of each phase

(liquid phase and solid phase) to total bacterial decrease during the photodegradation process. We anticipate this model to be a starting point for the development of a numerical tool for scaling up efficient photocatalytic reactors using immobilized photocatalytic media and solar light. Moreover, as photocatalytic bacterial inactivation is a promising technology for tertiary treatment of wastewaters, the optimization of bacteria–catalyst interactions, and the subsequent disinfection process is a critical issue.

Literature Cited

1. Pham HN, McDowell T, Wilkins E. Photocatalytically mediated disinfection of water using TiO_2 as a catalyst and spore forming *Bacillus pumulus* as a model. *J Environ Sci Health A*. 1995;30:627–636.
2. Block SS, Seng VP, Goswami DW. Chemically enhanced sunlight for killing bacteria. *J Sol Energy Eng*. 1997;119:85–91.
3. Bekbölet M. Photocatalytic bactericidal activity of TiO_2 in aqueous suspensions of *E. coli*. *Water Sci Technol*. 1997;35:95–100.
4. Munoz I, Rieradevall J, Torrades F, Peral J, Domènech X. Environmental assessment of different solar driven advanced oxidation processes. *Sol Energy*. 2005;79:369–375.
5. Malato S, Fernandez-Ibanez P, Maldonado MI, Blanco J, Gernjak W. Decontamination and disinfection of water by solar photocatalysis: recent overview and trends. *Catal Today*. 2009;147:1–59.
6. Otaki M, Hirata T, Ohgaki S. Aqueous microorganisms inactivation by photocatalytic reaction. *Water Sci Technol*. 2000; 42:103–108.
7. Guillard C, Bui T.H, Felix C, Moules V, Lina B, Le jeune P. Microbiological disinfection of water and air by photocatalysis. *C R Chim.* 2008;11:107–113.
8. Peller JR, Whitman RL, Griffith S, Harris P, Peller C, Scalzitti J. TiO_2 as a photocatalyst for control of the aquatic invasive alga, *Cladophora*, under natural and artificial light. *J Photochem Photobiol A*. 2007;186:212–217.
9. Sichel C, de Cara M, Tello J, Blanco J, Fernández-Ibáñez P. Solar photocatalytic disinfection of agricultural pathogenic fungi: *Fusarium* species. *Appl Catal B*. 2007;74:152–160.
10. McCullagh C, Robertson J.M.C, Bahnemann D.W, Robertson P.K.J. The application of TiO_2 photocatalysis for disinfection of water contaminated with pathogenic micro-organisms: a review. *Res Chem Intermed*. 2007;33:359–375.
11. Chick H. An investigation of the laws of disinfection. *J Hyg*. 1908; 8:92–158.
12. Cho M, Chung H, Yoon J. Disinfection of water containing natural organic matter by using ozone-initiated radical reactions. *Appl Environ Microbiol*. 2003;69:2284–2291
13. Marugán J, van Grieken R, Sordo C, Cruz C. Kinetics of the photocatalytic disinfection of *Escherichia coli* suspensions. *Appl Catal B*. 2008;82:27–36.
14. Dalrymple OK, Stefanakosa E, Trotzb MA, Goswami DY. A review of the mechanisms and modeling of photocatalytic disinfection. *Appl Catal B*. 2010;98:27–38.
15. Pablos C, van Grieken R, Marugán J, Chowdhury I, Walker SL. Study of bacterial adhesion onto immobilized TiO_2: effect on the photocatalytic activity for disinfection applications. *Catal Today*. 2013;209:140–146.
16. Correia F, Goetz V, Plantard G, Sacco D. A model for solar photocatalytic mineralization. *J Sol Energy Eng*. 2011;133:1–5.
17. Plantard G, Janin T, Goetz V, Brosillon S. Solar photocatalysis treatment of phytosanitary refuses: efficiency of industrial photocatalysts. *Appl Catal B*. 2012;115–116:38–44.
18. Pigeot-Remy S, Simonet F, Errazuriz-Cerda E, Lazzaroni JC, Atlan D, Guillard C. Photocatalysis and disinfection of water: identification of potential bacterial targets. *Appl Catal B*. 2011;104:390–398.
19. NF EN ISO 9308-3 (T 90-433). Mars 1999. Qualité de l'eau. Recherche et dénombrement des Escherichia coli et des bactéries coliformes dans les eaux de surface et résiduaires. Partie 3: Méthode miniaturisée (nombre le plus probable) pour ensemencement en milieu liquide. France: AFNOR.
20. Goetz V, Cambon JP, Sacco D, Plantard G. Modeling aqueous heterogeneous photocatalytic degradation of organic pollutants with immobilized TiO_2. *Chem Eng Process: Process Intensif*. 2009;48:532–537.
21. Kacem M, Plantard G, Wery N, Goetz V. Kinetics and efficiency displayed by supported and suspended TiO_2 catalysts applied to the disinfection of *Escherichia coli*. *Chin J Catal*. 2014;35:1571–1577.
22. Kalogirou S. Design, construction, performance evaluation and economic analysis of an integrated collector storage system. *Renew Energy*. 1997;12:179–192.
23. Fernández-Ibáñez P, Blanco J, Malato S, de las Nieves FJ. Application of the colloidal stability of TiO_2 particles for recovery and reuse in solar photocatalysis. *Water Res*. 2003;37:3180–3188.
24. Malato S, Blanco J, Maldonado MI, Fernandez-Ibanez J, Padilla DA, Pereira MC, Mendes JF, Correia de Oliveira J. Engineering of solar photocatalytic collectors. *Sol Energy*. 2004;77:513–524.
25. Guillard C, Bui TH, Felix C, Moules V, Lina B, Lejeune P. Microbiological disinfection of water and air by photocatalysis. *C R Chim.* 2007;15:1–7.
26. Liu HL, Yang TCK. Photocatalytic inactivation of *Escherichia coli* and *Lactobacillus helveticus* by ZnO and TiO_2 activated with ultraviolet light. *Process Biochem*. 2003;39:475–481.
27. Won J, Kim JW, Kang S, Choi H. Transport and adhesion of *Escherichia coli* JM109 in soil aquifer treatment (SAT): one dimensional column study. *Environ Monit Assess*. 2007;129:9–18.
28. Liu Y, Huang J, Ding S, Liu Y, Yuan J, Li H. Deposition, characterization, and enhanced adherence of *Escherichia coli* bacteria on flame-sprayed photocatalytic titania-hydroxyapatite coatings. *J Therm Spray Technol*. 2013;22:1053–1062.
29. Hijnen WAM, Suylen GMH, Bahlman JA, Brouwer-Hanzens A, Medema GJ. GAC adsorption filters as barriers for viruses, bacteria and protozoan (oo) cysts in water treatment. *Water Res*. 2010;44: 1224 –1234.
30. Berney M, Weilenmann HU, Ihssen J, Bassin C, Egli T. Specific growth rate determines the sensitivity of *Escherichia coli* to thermal, UV and solar disinfection. *Appl Environ Microbiol*. 2006;72:2586–2593.
31. Benabbou AK, Derriche Z, Felix C, Le jeune P, Guillard C. Photocatalytic inactivation of *Escherischia coli*. Effect of concentration of TiO_2 and microorganism, nature and intensity of UV irradiation. *Appl Catal B*. 2007;76:257–263.
32. Bayarri B, Abellàn MN, Gimenez J, Esplugas S. Study of the wavelength effect in the photolysis and heterogeneous photocatalysis. *Catal Today*. 2007;129:231–239.
33. Emeline AV, Ryabchuk V, Serpone N, Factors affecting the efficiency of a photocatalysed process in aqueous metal-oxide dispersions. *Prospect of distinguishing between two kinetic models*. *J Photochem Photobiol A*. 2000;133:89–97.
34. Li Puma G, Yue PL. A laminar falling film slurry photocatalytic reactor. Part 1– model development. *Chem Eng Sci*. 1998;53:2993–3006.
35. Turchi CS, Ollis DF. Photocatalytic degradation of organic water contaminants: mechanisms involving hydroxyl radical attack. *J Catal*. 1990;122:178.
36. Thiebaud J, Thevent F, Fittschen C. OH radicals and H_2O_2 molecules in the gas phase near to TiO_2 surfaces. *J Phys Chem C*. 2010; 114:3082–3088.
37. Lee MC, Choi W. Solid phase photocatalytic reaction on the soot/TiO_2 interface: the role of migrating OH radicals. *J Phys Chem B*. 2002;106:11818–11822.
38. Matsunaga T, Tomoda R, Nakajima T, Wake H. Photoelectrochemical sterilization of microbial cells by semiconductor powders. *FEMS Microbiol Lett*. 1985;29:211–214.
39. Mills A, Le Hunte S. An overview of semiconductor photocatalysis. *J Photochem Photobiol A*. 1997;108:1–35.
40. Murakami Y, Kenji E, Nosaka AY, Nosaka Y. Direct detection of OH radicals diffused to the gas phase from the UV-irradiated photocatalytic TiO_2 surfaces by means of laser-induced fluorescence spectroscopy. *J Phys Chem B*. 2006;110:16808–16811.
41. Ollis DF. Kinetics of liquid phase photocatalyzed reactions: an illuminating approach. *J Phys Chem B*. 2005;109:2439–2444.
42. Mills A, Wang J, Ollis DF. Kinetics of liquid phase semiconductor photo assisted reactions: supporting observations for a pseudo-steady-state model. *J Phys Chem B*. 2006;110:14386–14390.
43. Yang RT. Gas separation by adsorption processes. In: Gas separation by adsorption processes. Brenner H, editor. Boston: Butterwoorth; 1987:101–139.
44. Barker JJ, Treybal RE. Mass transfer coefficient for solids suspended in agitated liquids. *AIChE J*. 1960;2:289–295.
45. Guo L, Jury WA, Wagenet RJ, Flury M. Dependence of pesticide degradation on sorption:nonequilibrium model and application to soil reactors. *J Contam Hydrol*. 2000;43:45–62.

Appendix

See Figures A1–A4.

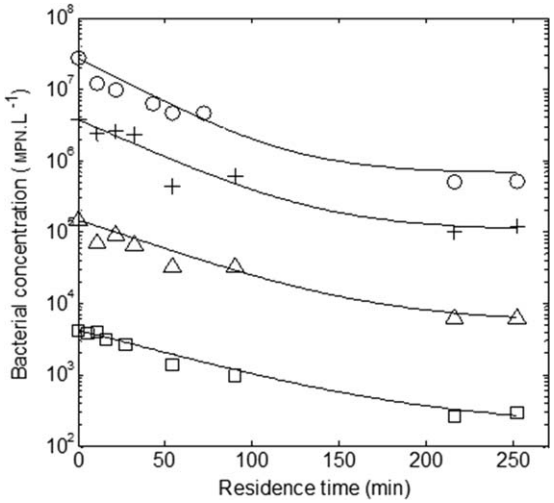

Figure A1. Adhesion kinetics of *E. coli* over residence time using the suspended VP Aeroperl catalyst and for different initial bacterial concentrations.

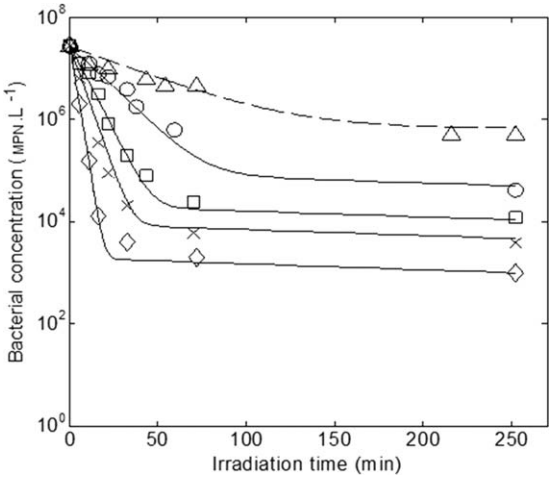

Figure A3. Experimental and simulated results of the photocatalytic inactivation of *E. coli* over irradiation time using the suspended VP Aeroperl catalyst under variable irradiation flux densities

0 W m^{-2} (Δ), 5 W m^{-2} (○), 10 W m^{-2} (□), 20 W m^{-2} (×), and 35 W m^{-2} (◇).

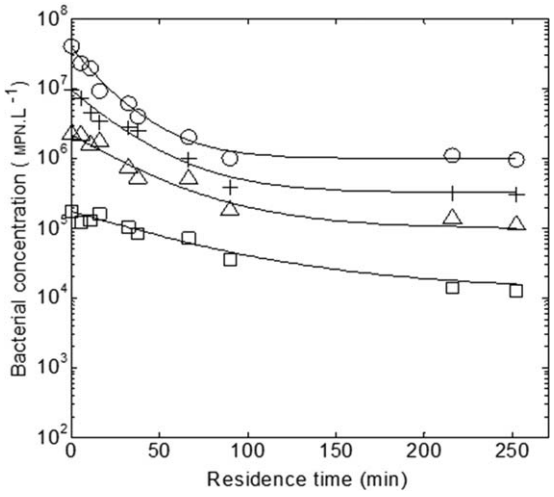

Figure A2. Adhesion kinetics of *E. coli* over residence time using the supported catalyst and for different initial bacterial concentrations.

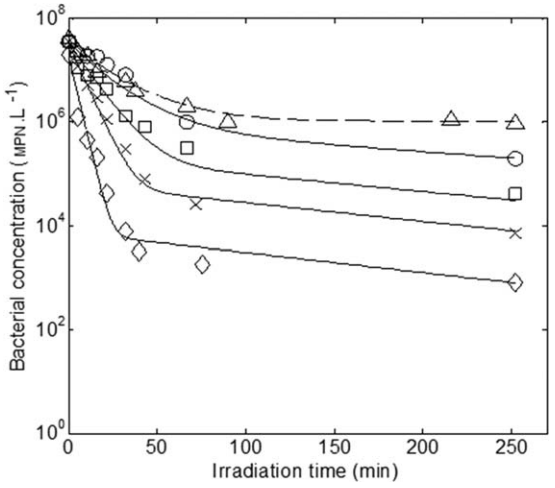

Figure A4. Experimental and simulated results of the photocatalytic inactivation of *E. coli* over irradiation time using the supported catalyst under variable irradiation flux densities

0 W m^{-2} (Δ), 5 W m^{-2} (○), 10 W m^{-2} (□), 20 W m^{-2} (×), and 35 W m^{-2} (◇).

Manuscript received Oct. 27, 2014, and revision received Feb. 23, 2015.